Experimental Mechanics (2007) 47: 37–49
DOI 10.1007/s11340-006-0405-7

Elastic Properties and Representative Volume Element of Polycrystalline Silicon for MEMS

S.W. Cho · I. Chasiotis

Received: 12 February 2006 / Accepted: 15 September 2006 / Published online: 2 December 2006

Abstract A nanoscale mechanical deformation measurement method was employed to obtain the Young's modulus and Poisson's ratio of polycrystalline silicon for Microelectromechanical Systems (MEMS) from different facilities, and to assess the scale at which these effective properties are valid in MEMS design. The method, based on *in situ* Atomic Force Microscope (AFM) imaging and Digital Image Correlation (DIC) analysis, employed 2–2.5 μm thick freestanding specimens with surface measurement areas varying between 1×2 and 5×15 μm^2. The effective mechanical properties were quite invariant with respect to the fabrication facility: the Poisson's ratio of polycrystalline silicon from the Multi-user MEMS Processes (MUMPs) and from Sandia's Ultra planar four layer Multilevel MEMS Technology (SUMMiT-IV) was 0.22 ± 0.02, while the elastic moduli for MUMPs and SUMMiT-IV polysilicon were 164 ± 7 and 155 ± 6 GPa, respectively. The AFM/DIC method was used to determine the size of the material domain whose mechanical behavior could be described by the isotropic constants. For SUMMiT polysilicon with columnar grains and 650 nm average grain size, it was found that a 10×10-μm^2 specimen area, on average containing 15×15 columnar grains, was a representative volume element. However, the axial displacement fields in 4×4 or 2×2 μm^2 areas could be highly inhomogeneous and the effective behavior of these specimen domains could deviate significantly from that described by isotropy. As a consequence, the isotropic material constants are applicable to MEMS components comprised of 15×15 or more grains, corresponding to specimen areas equal to 10×10 μm^2 for SUMMiT and 5×5 μm^2 for MUMPs, and do not provide an accurate description of the mechanics of smaller MEMS components.

Keywords Nanoscale mechanics · AFM · Digital image correlation · Polysilicon

S.W. Cho
Materials Science and Engineering,
University of Virginia,
Charlottesville, VA 22904, USA

I. Chasiotis (✉, SEM Member)
Aerospace Engineering,
University of Illinois at Urbana–Champaign,
Urbana, IL 61801, USA
e-mail: chasioti@uiuc.edu

Introduction

The ability to fabricate micron-size components for Microelectromechanical Systems (MEMS) led to the demand for mechanical properties for device modeling and calibration. In addition to metrological uncertainties pertaining to the precise device geometry and dimensions that weaken our ability to predict the accurate mechanical behavior of small MEMS components, the local microstructural details are equally important, especially when component and material grain sizes are of the same order of magnitude. In this regard, elastic deformations may be described in statistical terms or be determined numerically from knowledge of the exact grain structure. The latter approach, however, is impractical due to the large number of

geometrically identical sensors and actuators fabricated on a single silicon chip.

To date, polycrystalline silicon (polysilicon) is the material of choice for the fabrication of most MEMS devices. It is considered modestly anisotropic with a modulus varying between $130.2 < E < 187.9$ GPa in [100] and [111] directions, respectively [1]. Films with 1-μm or larger thickness are usually comprised of relatively columnar grains with 300–600 nm average grain size that depends on the fabrication method. This microstructure permits large polysilicon components to be considered as transversely isotropic and under plane strain, locally and globally.

To date, thin film mechanical testing methods developed for MEMS-scale specimens provided the Young's modulus (a detailed review is given in [1]) while very few methods measured both elastic constants directly from microscale specimens. First, Sharpe et al. [2] reported the Poisson's ratio of polysilicon using 0.6-mm wide and 4-mm long specimens and interferometric displacement measurements. At the scale of a few millimeters, membrane deflection tests with a combination of square and rectangular membranes were conducted to obtain the isotropic properties of polysilicon [3] following a method by Vlassak and Nix [4]. At scales comparable to the grain size, the only report with direct measurements of Poisson's ratio and Young's modulus is by Cho et al. [5] who employed full-field nanoscale displacement measurements and the linear elasticity solution to the inverse problem of a 6-μm central hole in a 60-μm wide specimen subject to uniaxial tension. Nanoscale deformations were derived from 15×15-μm^2 Atomic Force Microscope (AFM) images at the root of the central hole by the application of Digital Image Correlation (DIC) method.

These isotropic properties are valid for a large aggregate of grains, such as MEMS devices that are tens to hundreds of microns large. However, polycrystalline anisotropy can be important when the lateral dimensions of a device are comparable to the columnar grain diameter. For film thicknesses larger than 1,000 nm, the grain diameter remains approximately the same and independent of the device geometry that is determined by photolithographic patterning of blanket films. If the isotropic properties were used for a MEMS component comprised of a few grains, its predicted effective mechanical behavior would deviate from the true behavior [6]. It is thus important to identify the scale limits in the application of isotropic elastic constants and specifically, the representative volume element (RVE) of polysilicon, i.e., the minimum material volume that behaves isotropically. In this work the RVE was determined according to the definition by Drugan and Willis [7] as the minimum specimen size whose overall mechanical behavior under tension could be described by the Young's modulus measured from a macroscopically homogenous sample of the same material. The AFM/DIC method was employed to determine the size of the RVE for polysilicon in an analogy to prior works that conducted optical measurements to compute the size of an RVE of particulate composites [8].

In this paper the effective properties of polycrystalline silicon were obtained from directly measured axial and transverse full-field displacements with nanoscale spatial resolution of about 2 nm. The experimental approach employed micron size freestanding specimens and direct records of the local nanoscale deformations. We report for the first time the elastic constants of polysilicon films for MEMS from two fabrication facilities for which not all properties have been obtained before. Furthermore, the validity of these properties in the design and modeling of small MEMS components is established by applying the AFM/DIC method at various physical scales to determine the size of the RVE for polysilicon.

Experimental Details

Polysilicon samples were manufactured at two established MEMS fabrication facilities using the Multi-user MEMS Processes (MUMPs) [9] and the Sandia Ultra planar four layer Multilevel MEMS Technology (SUMMiT IV) process [10] to ensure good film quality, small defect density, and dimensional accuracy. Although there is a detailed account of Young's modulus measurements and three reports on Poisson's ratio for MUMPs [2, 3, 5], limited information is available about the elastic modulus and none about Poisson's ratio for SUMMiT polysilicon. Furthermore, there is no comparative study of the mechanical properties of polysilicon from the two processes using the same experimental method, while the applicability of these effective properties to components whose size is only a few microns is unknown.

Specimen Fabrication

The specimens were surface micromachined tensile structures attached to a silicon chip. Their gage sections were of the scale of common MEMS components, i.e., 2–2.5 μm thick, 20–50 μm wide, and 500–1,000 μm long. They were fabricated at Cronos in North Carolina by the MUMPs 41 run and at Sandia National Laboratories (SNL) in New Mexico by the SUMMiT-IV process.

The surface characteristics of the two types of polysilicon were different: The average surface roughness of SUMMiT polysilicon was 10 nm, while the average roughness of MUMPs polysilicon was 25 nm. The surface roughness, although important in the determination of the material strength, is not key in the calculation of the elastic properties unless it is considerable and affects the accurate determination of the specimen thickness.

The MUMPs specimens were 2 μm thick fabricated by Low-Pressure Chemical Vapor Deposition (LPCVD) on a 2-μm thick Phosphosilicate Glass (PSG) layer. This layer was the first structural layer (poly1) of the MUMPs process. This polycrystalline silicon was diffusion-doped with phosphorous and was annealed at 1,050°C for 1 h to reduce residual stresses and provide adequate doping (and thus electrical conductivity). The chips (dies) were released by 49% wt. HF wet etch and were dried by CO_2 supercritical point drying (CPD). Further processing details are provided in [9]. The grain structure of MUMPs polysilicon has been reported to be columnar with relatively uniform grain diameter across most of the film thickness and dominant <110> texture [3]. The average grain size, as measured at the top film surface with an AFM and via the mean linear intercept method, was 320 ± 25 nm where 25 nm was the standard deviation.

The specimens fabricated by SUMMiT-IV, were 2.5 μm thick as a result of the combination of the poly1 and poly2 layers. They were fabricated from silane, n-doped with Phosphine gas [11] and were annealed at 1,100°C to reduce residual stresses [12]. Finally, they were released by 90 min exposure to 1:1 HF:H_2O solution and dried by CPD [13]. The grain size of the SUMMiT polysilicon measured from AFM surface images was 650 ± 50 nm with considerable spread in values. As reported in [14], this polysilicon has no preferred texture.

The specimens were dog-bone in shape similar to those used by this group before [15]. They were freestanding, thus eliminating the need to account for substrate effects that are common with other methods, such as nanoindentation and testing of thin films deposited on deformable substrates.

Test Apparatus

The loading apparatus was based on the method developed by Chasiotis and Knauss [15] that makes use of a viscous Ultraviolet (UV) light curable adhesive and a flat glass grip to conduct MEMS testing. This method facilitates the *in situ* use of an AFM to obtain specimen images during loading and deduce local mappings of mechanical deformation. Figure 1 shows the process of gripping the large specimen pedal ($600 \times 1{,}200$ μm^2) and applying load by a flat glass grip cut from a glass slide. The global displacement on the specimen was imposed by a piezoelectric actuator with 4 nm resolution. The induced load was measured with a miniature tension/compression load cell with 500 μN accuracy. This micro-tensile test apparatus is described in detailed in [16].

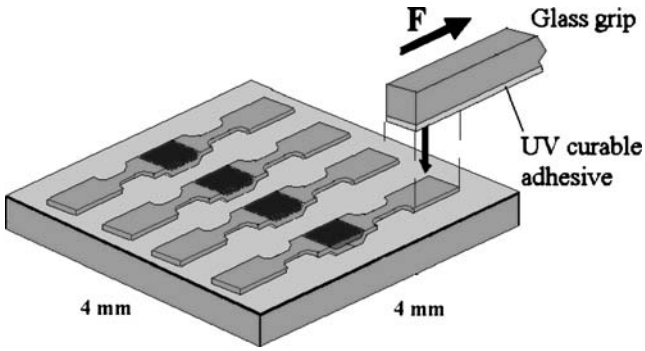

Fig. 1 Specimen layout on silicon chip and loading method using a glass grip coated with UV curable adhesive

Important instrumentation requirement was the hardware linearization of the AFM piezoelectric actuator which commonly is subject to several non-linearities. A hardware correction of the PZT actuator was required for both the x and the y coordinates. On the other hand, the z-axis (height) data were not used to determine out-of-plane deformations and small uncertainties in the out-of-plane measurements were not as important. Such small uncertainties that were present in addition to noise were accounted for by the addition of an arbitrary offset in the construction of the least-square coefficient that was used in the minimization routine of the DIC algorithm. The z-linearization hardware was inactive for the smallest AFM scans presented here in order to improve the signal-to-noise ratio. An additional consideration was the rigid body motion of the AFM field of view with regards to the specimen at each load increment. In order to relocate the area of interest, the test apparatus was placed on a translation stage with submicron positioning accuracy so that a near zero offset was applied to the AFM piezoelectric actuator in the x and y directions after each increment of applied stress.

The MEMS specimens were of the same, or larger, thickness as the AFM cantilevers that were used for AFM imaging. The AFM was operated in non-contact mode to minimize the bending force exerted on the specimen by the AFM cantilever during imaging. The minimum nominal radius of curvature of the cantilever tip was 10 nm. It was fabricated by Si or Si_3N_4 with the latter proven to be more robust and resistant to wear.

Special care was taken so that the same tip, or tips of the same radius, were used throughout imaging so that tip broadening effects were minimized.

Full-Field Nanoscale Deformation Measurements

The material deformations were deduced from AFM images by the application of DIC. The method calculates in-plane displacements by comparing (surface) records of the same physical area obtained at different load levels. Although the hardware resolution is limited to deformations that amount to integer multiples of an image pixel, the use of non-linear bicubic spline interpolation permits the calculation of local sub-pixel displacements. The method, initially developed for optical imaging [17], has been used with AFM data [5, 15, 16] that are digital in nature and facilitate its direct application to determine strain fields. A speckle pattern is required for the implementation of DIC. When AFM images are employed this pattern is provided by the natural surface roughness features that act as distributed markers. In polycrystalline silicon the major contribution to the surface pattern comes from grain boundaries and from the intra-grain surface roughness that is of small amplitude. A description of the mathematical formulation and an analysis of the limitations of the DIC method as a function of surface features and data noise are given in [18].

DIC has been shown to calculate displacements with an accuracy of about 1/8 of an image pixel [18], which implies that strains smaller than 0.02% could be resolved with the current state-of-the-art AFM instrumentation with $1{,}024 \times 1{,}024$ pixel resolution. The method simultaneously calculates in-plane displacements and their gradients via a least-squares optimization. The calculation of displacements is more accurate than their gradients and thus the former are presented in this paper without the application of noise filters. Temperature fluctuations, ambient noise, and vibrations limit the accuracy of nanoscale displacements computed from AFM images. Thermal drift is a significant contributor to image distortions and as a rule of thumb, the room temperature during AFM imaging should be maintained within a tenth of a degree centigrade, while ambient accelerations must be smaller than 50 μg.

The effective engineering strain was determined in two ways: from (a) the cross-head displacements, and (b) the full-field displacements in the mid-section of the specimen resolved by AFM/DIC. In the first approach, the contribution of the test system compliance was measured and the elastic modulus was calculated by a finite element model of the specimen to account for the deformation of its non-uniform segments and the compliance of the apparatus. In the second mode, the axial and transverse displacement fields were measured by the AFM/DIC method. Depending on the selected field of view, the total displacement in the axial direction ranged from 20–200 nm. The total transverse displacement in the entire field of view due to the Poisson's effect was only in the range of 10–50 nm.

The application of DIC took into consideration the procedure of AFM data collection in order to accurately resolve the spatial distribution of nanometer scale displacements from AFM images. Ideally, a pair of AFM images contains sufficient information to extract the u and v displacements in the x and y directions, respectively. However, one should take into account the fact that the AFM collects data by rastering a cantilever along a straight line in the x-direction (called the fast scanning direction) in 1 s, or less, collecting 1,024 equally spaced surface height readings. Subsequently, the cantilever moves in the y-direction (called the slow scanning direction) to the next image line, repeats a fast scan of one line along the x-direction and continues until it collects 1,024 slow scanning lines. Considering that thermal effects are important over times quite longer than 1 s, the data obtained in the fast scanning direction are rather insensitive to temperature fluctuations and thus more accurate than the data in the slow scanning direction. To increase the fidelity of the AFM images used in DIC, two image sets were collected at each applied load with x and y as the fast scanning directions. Then, the u and v displacements were calculated from AFM images collected with x and y as the fast scanning direction, respectively. In each case the direction of fast imaging was aligned with, or was normal to, the specimen loading axis.

Results and Discussion

Effective Mechanical Behavior

A stress–strain curve obtained from the cross-head displacement and the apparatus stiffness as inputs to a FE model of the SUMMiT-IV polysilicon specimens is shown in Fig. 2. The elastic modulus of this specimen was 160.6 GPa. The specimens fabricated by SUMMiT-IV demonstrated the highest tensile strength averaging 3.1 GPa. The stress–strain behavior was linearly elastic until failure at tensile strains over 2%. Similarly, the stress–strain curve measured from MUMPs

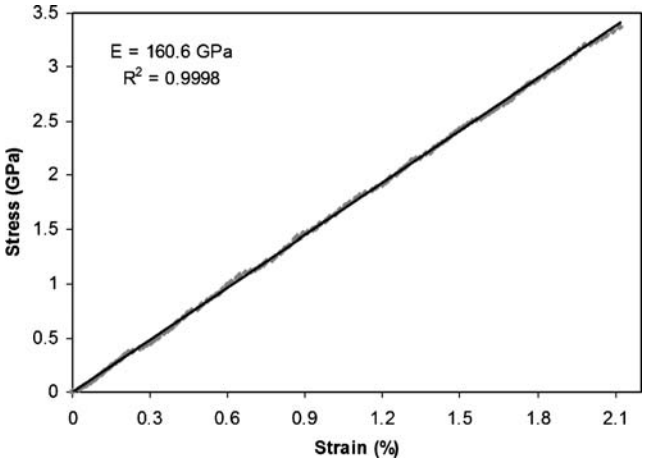

Fig. 2 Engineering stress–strain curve for SUMMiT polysilicon. A *straight line* is fit to the experimental data points

specimens was also linear until failure at strains averaging 1.2% and 1.8 GPa tensile strength.

The local deformation measurements were obtained by the AFM/DIC method. The application of DIC is conducted pointwise and the displacements at each material point are computed with the aid of a correlation square surrounding the correlation point. The former is used to generate a continuous surface from a discrete set of data points. This correlation square must include sufficient surface features so that it is uniquely matched to an area in the deformed image. Since the speckle pattern was provided by the details of the grain boundaries and in part by the intragrain roughness, the pixel size of the correlation square was dictated by the physical size of the entire image. The correlation square used to calculate the effective properties in the 5×15-μm^2 AFM images was 20×20 pixels (300×300 nm). The optimum size of the correlation square was determined iteratively. Small sizes that did not contain sufficient surface details resulted in erroneous local displacements while very large correlation squares resulted in smooth displacement contours eliminating local information.

A set of five AFM images was obtained at each of the five or more load levels applied to every specimen. Figure 3 shows a sequence of axial and transverse displacement contours and the applied stresses. The contour legends were adjusted to the maximum displacement range that was recorded at the highest load. The u and v displacements were obtained from AFM images with fast scanning directions along the x- and the y-axis, respectively. The axial and transverse displacements were quite uniform in 5×15-μm^2 fields sampled at different locations on the specimen, which is expected for a uniaxial tension test. Thus, polysilicon specimens of this size behave isotropically and in a linearly elastic manner. As will be verified later, a 15×15-μm^2 specimen area is an RVE for polysilicon.

The average axial and transverse strains at each applied stress were obtained as the average slope of all horizontal contour lines in Fig. 3. Two line fits from the axial and transverse displacement contours at 2.5 GPa applied stress in Fig. 3 are shown in Fig. 4. For a linearly elastic material the local displacement as a function of position yields a straight line whose slope du/dx is the line strain. The calculation of the average strain by this approach was more consistent compared to the local du/dx computed by DIC, or by point-by-point differentiation of the displacement field. Averaging of the latter full-field strains could remove the random noise and provide a uniform strain at each load level but the displacement data required smoothing that would make this analysis subjective.

The average axial strain for each contour was obtained from the line fits to the displacement data. Subsequently, the strains from 25 contour images per load level were averaged. It should be noted that when optical microscopy is used it is customary to average the undeformed and the deformed images before conducting DIC so that fluctuations in the pixel gray level intensity are minimized. This is not possible with AFM images because of the small rigid body displacements that occur between consecutive images.

Knowledge of the average strain at each load helped to construct the stress–strain curves such as that shown in Fig. 5. The stress was the nominal stress calculated from the force readings of the load cell. Although the number of points was small due to the time required for AFM imaging, all points fit a straight line very well whose slope provided the Young's modulus. The average elastic modulus for MUMPs 41 was 164 ± 7 GPa which agreed well with the value of 165.7 GPa reported before [15] using global measurements that accounted for the apparatus compliance. Similar values have been published about MUMPs by other researchers [2, 3]. The elastic modulus of SUMMiT polysilicon was 155 ± 6 GPa, which is in good agreement with the effective modulus of 164 ± 3 GPa reported in [14]. On the other hand, the Poisson's ratio has not been reported before for both processes or obtained at this scale. Using the full-field axial and transverse deformation data, the Poisson's ratio was found to be virtually the same for both processes averaging 0.219 ± 0.018 and 0.224 ± 0.017 for MUMPs and SUMMiT-IV, respectively. These values agree with measurements conducted on MUMPs polysilicon at the same scale using inverse solutions to deduce the elastic properties [5], and with the average properties reported

in [2] where the relative displacements of surface markers spaced 200 μm apart were recorded by an interferometric method.

Table 1 summarizes the experimental results. The difference in the elastic properties between the two processes was on the order of 5% or less, while the mechanical strength differed by as much as 60% with the SUMMiT-IV results taken as reference. The large deviation in strength was attributed to the high surface roughness of MUMPs polysilicon that generated distributed surface notches. The strength values reported here are for MUMPs specimens with no Au

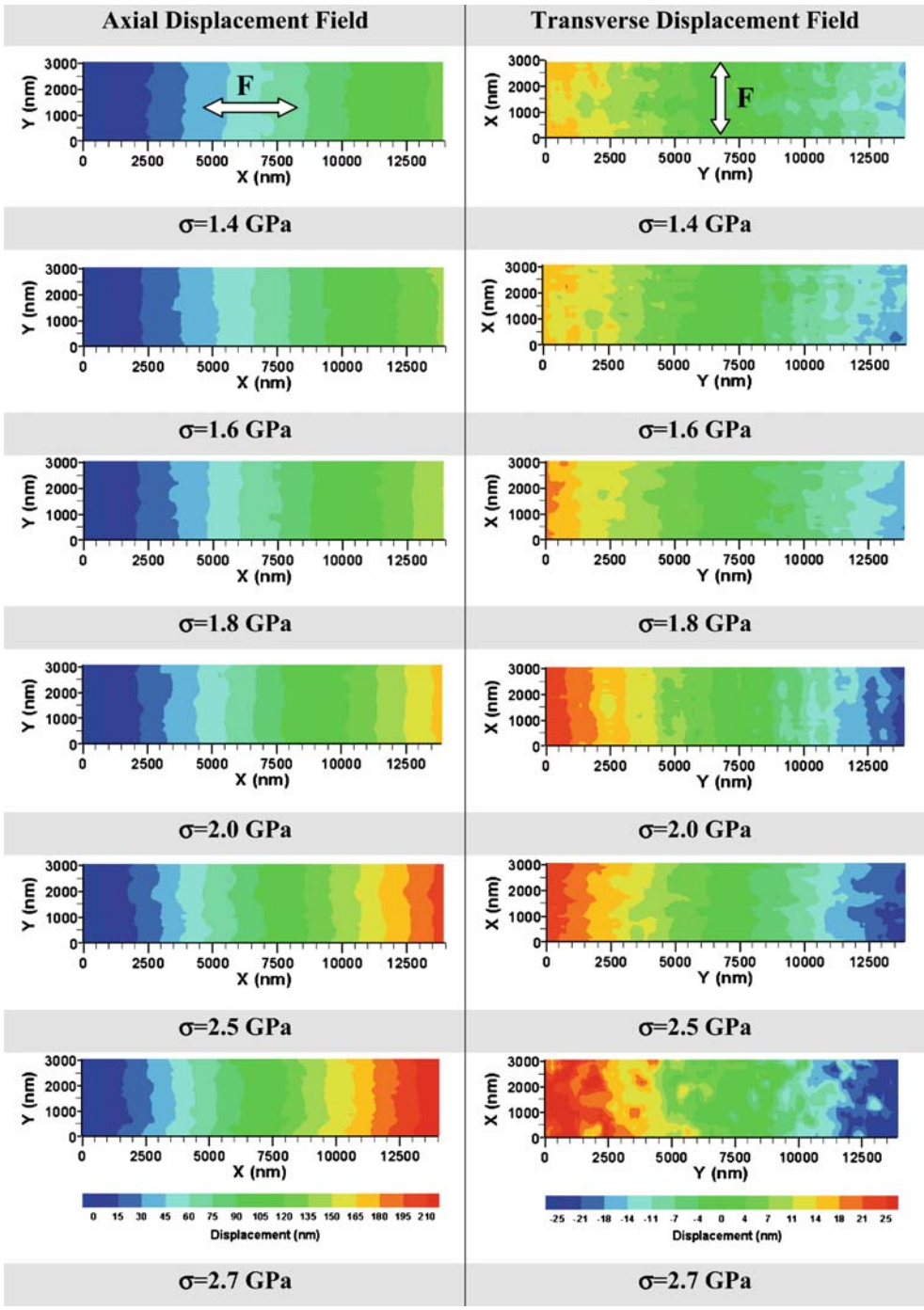

Fig. 3 Axial and transverse displacement fields in a 15×15-μm^2 specimen area from SUMMiT polysilicon. The *left-to-right* order of *gray levels* in the axial displacement contours is the same as in the contour legend, and the opposite is true for the transverse displacement contours. Images are best viewed in color

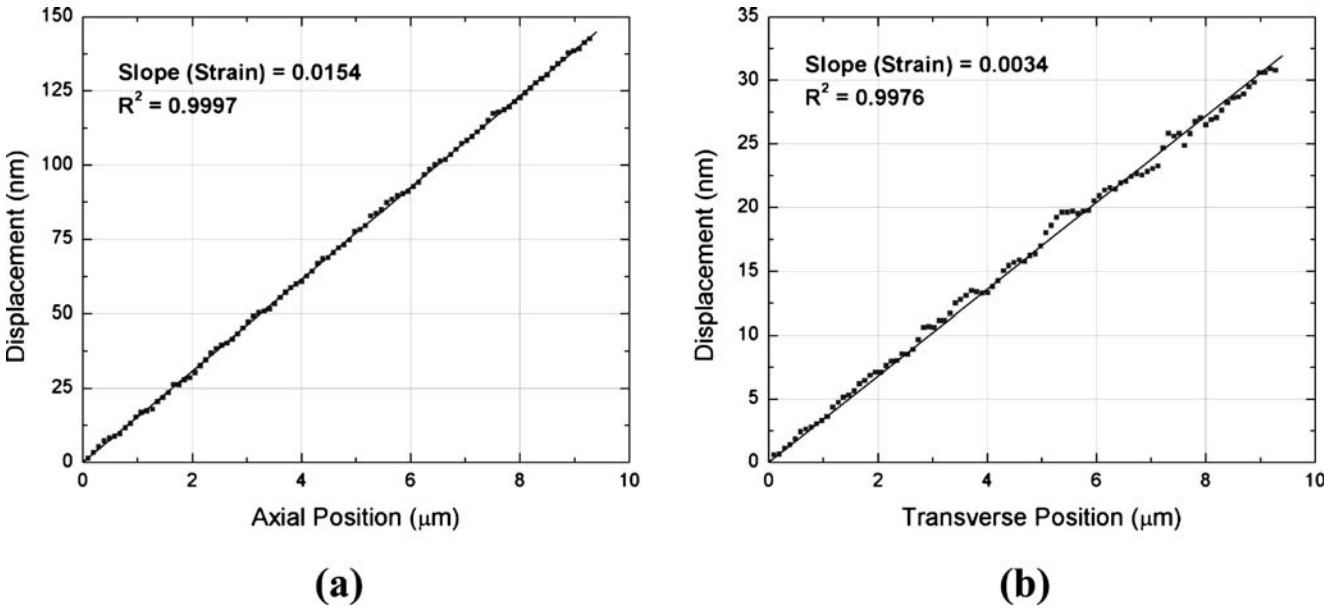

Fig. 4 Local displacement as a function of position in the (**a**) axial and (**b**) transverse direction, respectively. The data lines were derived from the contours in Fig. 3 at 2.5 GPa applied stress

layer. As a result, they were considerably higher compared to previous reports [19] where the Au layer generated undesirable surface conditions after HF processing. Similarly, no metallization was present on the SUMMiT-IV polysilicon.

Comparison of Effective Properties with Analytical Estimates

The experimental properties in Table 1 may be compared to those calculated using crystal elasticity.

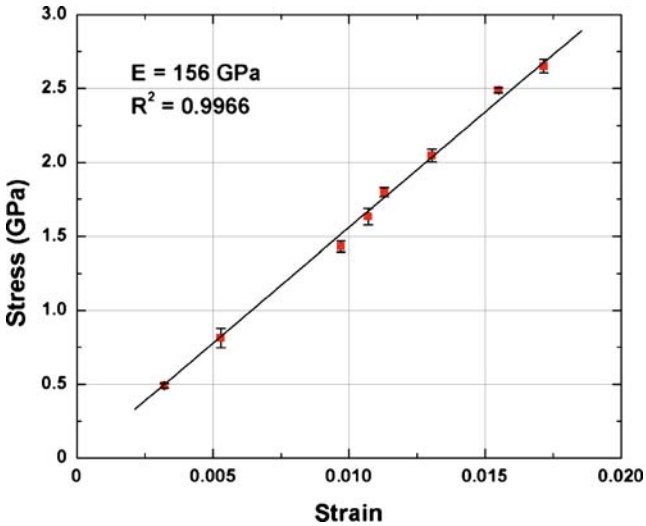

Fig. 5 Stress–strain curve calculated from the displacement contours in Fig. 3. Each point is the average of the strain measured from 25 contour plots. The *error bars* for the strain measurements were too small to be shown

Both types of polysilicon had columnar grain structure but the MUMPs polysilicon had <110> texture while the SUMMiT polysilicon did not have a preferred texture [3, 14]. Although the columnar grain structure was not ideal, it could be used as a reasonable assumption to compute the elastic constants and their bounds.

The elastic modulus of single crystal silicon varies with the crystal direction as

$$E = \frac{1}{s_{11} - 2\left(s_{11} - s_{12} - \frac{s_{44}}{2}\right)\left(\alpha^2\beta^2 + \alpha^2\gamma^2 + \beta^2\gamma^2\right)} \tag{1}$$

where α, β and γ are the direction cosines and s_{ij} are the compliance coefficients [20]. The Poisson's ratio that measures the contraction in direction $n = (k,l,m)$ for an applied stress in direction $s = (\alpha,\beta,\gamma)$ is [20]

$$\nu = -\frac{s_{12} + \left(s_{11} - s_{12} - \frac{s_{44}}{2}\right)\left(\alpha^2k^2 + \beta^2l^2 + \gamma^2m^2\right)}{s_{11} - 2\left(s_{11} - s_{12} - \frac{s_{44}}{2}\right)\left(\alpha^2\beta^2 + \alpha^2\gamma^2 + \beta^2\gamma^2\right)} \tag{2}$$

The compliance coefficients, s_{ij}, for single crystal silicon are $s_{11} = 7.681\ \text{TPa}^{-1}$, $s_{12} = -2.138\ \text{TPa}^{-1}$, $s_{44} = 12.559\ \text{TPa}^{-1}$ [21]. Considering MUMPs polysilicon as transversely isotropic with <110> texture, equation (1) can be averaged for an aggregate of randomly oriented columnar grains to obtain an estimate for the effective in-plane modulus

$$\overline{E}_{<110>} = \frac{1}{2\pi}\int_{-\pi}^{\pi} 2\frac{d\theta}{2s_{11} - \left(s_{11} - s_{12} - \frac{1}{2}s_{44}\right)\cos^2(\theta)\left(1 + 3\sin^2(\theta)\right)} \tag{3}$$

Table 1 Elastic properties of MUMPs and SUMMiT-IV polycrystalline silicon

Fabrication process	Young's modulus (GPa)	Poisson's ratio	Tensile strength[1] (GPa)
SUMMiT-IV	155 ± 6	0.224 ± 0.017	3.09 ± 0.2
MUMPs 41	164 ± 7	0.219 ± 0.018	1.81 ± 0.1

[1] The tensile strength was measured from specimens with approximately the same gage section $1000 \times 20 \times 2$ μm^3 (L × W × T).

Similarly, the effective Poisson's ratio for <110> texture can be calculated from equation (2) as

$$\overline{v}_{<110>} = -\frac{1}{2\pi}\int_{-\pi}^{\pi} \frac{s_{12} + \frac{3}{8}\left(s_{11} - s_{12} - \frac{1}{2}s_{44}\right)\sin^2(2\theta)}{s_{11} - \frac{1}{2}\left(s_{11} - s_{12} - \frac{1}{2}s_{44}\right)\cos^2(\theta)(1+3\sin^2(\theta))}\mathrm{d}\theta \tag{4}$$

Substitution to equations (3) and (4) yields $\overline{E}_{<110>} = 165.5\ GPa$ and $\overline{v}_{<110>} = 0.239$. In the absence of texture, which is approximately the case for SUMMiT-IV polysilicon, the theoretical modulus is 163 GPa [14].

These effective properties compare well with the experimental results reported here. The actual microstructure of MUMPs polysilicon may deviate from that for <110> texture but the bounds for the elastic constants are very narrow even for a random grain orientation. Considering the isostrain Voigt model [22] the upper bounds for the elastic modulus and Poisson's ratio are given by

$$E_V = \frac{(c_{11} - c_{12} + 3c_{44})(c_{11} + 2c_{12})}{2c_{11} + 3c_{12} + c_{44}} \tag{5}$$

$$\nu_V = \frac{1}{2}\left(\frac{c_{11} + 4c_{12} - 2c_{44}}{2c_{11} + 3c_{12} + c_{44}}\right) \tag{6}$$

where c_{ij} are the stiffness coefficients. If isostress prevails, Reuss model [23], the lower bounds for the elastic modulus and Poisson's ratio are

$$E_R = \frac{5}{3s_{11} + 2s_{12} + s_{44}} \tag{7}$$

$$\nu_R = -\frac{1}{2}\left(\frac{2s_{11} + 8s_{12} - s_{44}}{3s_{11} + 2s_{12} + s_{44}}\right) \tag{8}$$

According to equations (5–8), the effective Young's modulus should lie between $160 < E < 166$ GPa and the effective Poisson's ratio between $0.218 < \nu < 0.228$; bounds that still agree with the measurements reported here. It should be noted that these bounds are appropriate for a sample comprised of a very large number of columnar grains so that the material can be considered as statistically homogeneous.

Local Mechanical Behavior

The elastic constants in Table 1 were obtained in 5×15-μm^2 specimen areas and were in agreement with the theoretical expectations and effective property measurements thus describing well the isotropic behavior of polysilicon. Due to grain inhomogeneity, these properties, although valid for specimen sizes 5×15 μm^2 or larger, may not appropriately describe the effective mechanical behavior of smaller specimen domains. Polycrystalline silicon is modestly anisotropic, $130.2 < E < 187.9$ GPa as calculated from equations (1) and (2) for [100] and [111] directions, respectively, but according to [6] when the specimen contains less than 200 grains crystalline anisotropy becomes important resulting in statistical variation of the effective properties. This numerical estimate of a minimum specimen size that behaves isotropically assumed columnar structure and <100> texture. Although the texture is not the same as that for MUMPs polysilicon, it provides a non-conservative first order estimate of the RVE for polysilicon.

The AFM/DIC method was applied to determine the smallest specimen size (RVE) whose effective mechanical behavior could be described by the isotropic properties of SUMMiT-IV polysilicon in Table 1. Because it was shown that a 15×15-μm^2 specimen is described well by these properties, smaller domain sizes were employed. Furthermore, the deviation from isotropy and inhomogeneity is of stochastic nature and it depends on the location on the sample. In this section one typical specimen area and one area that resulted in large deviation from homogeneity are presented. In both cases the structure of the material is assumed to be columnar which in general is considered to be a fair assumption. The first example involved six mutually inclusive domains with dimensions of $1 \times 2, 1.5 \times 3, 2 \times 4,$

Fig. 6 (*Left*) AFM images of (**a**) 5×10 μm^2, (**b**) 4×8 μm^2, (**c**) 3×6 μm^2, (**d**) 2×4 μm^2, (**e**) 1.5×3 μm^2, and (**f**) 1×2 μm^2 areas in a 2.5 μm thick polycrystalline silicon specimen subject to uniaxial tension. The areas marked by *rectangles* in (**a**–**e**) are images (**b**–**f**), respectively. The *small rectangle* in image (**a**) is image (**f**). All AFM images have 1,024 pixels per line resolution. (*Center*) *u*-displacements superposed on the grain structure. Contours are best viewed in color. (*Right*) Plots of the local *u*-displacement as a function of axial position. There is a direct correlation between local displacements and grain inhomogeneity for (**e**) 1.5×3 μm^2, and (**f**) 1×2 μm^2 areas

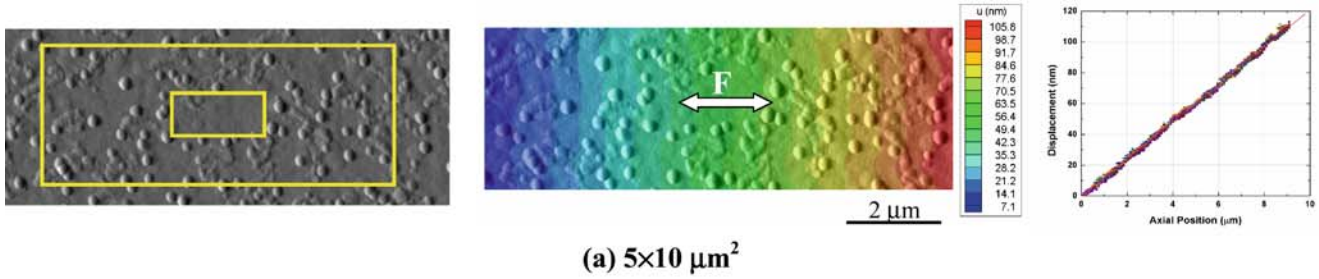

(a) 5×10 μm²

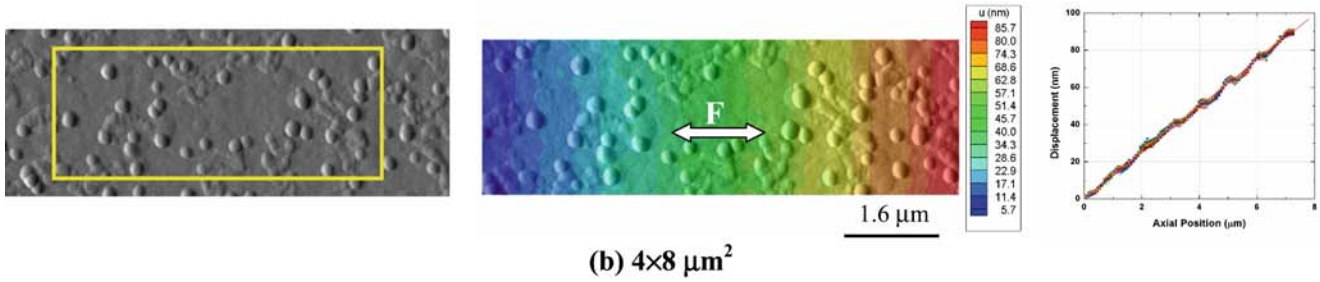

(b) 4×8 μm²

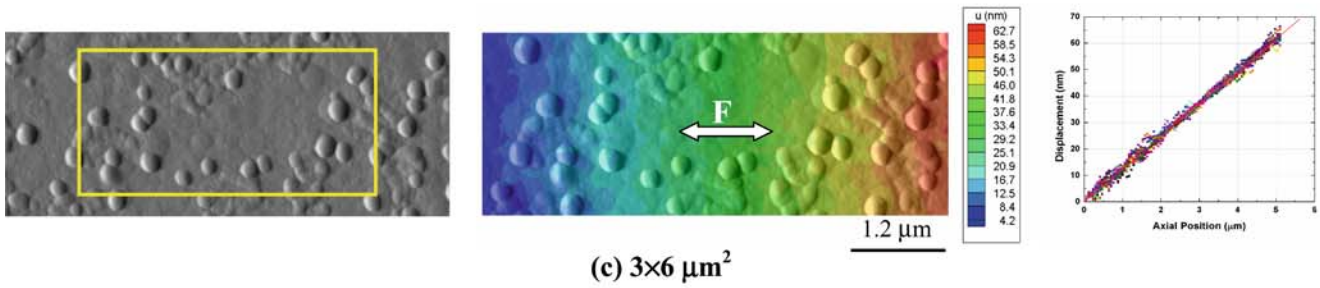

(c) 3×6 μm²

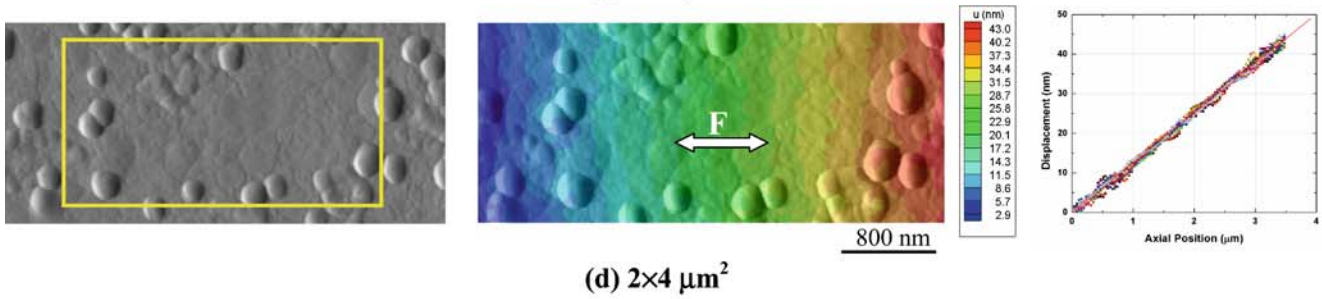

(d) 2×4 μm²

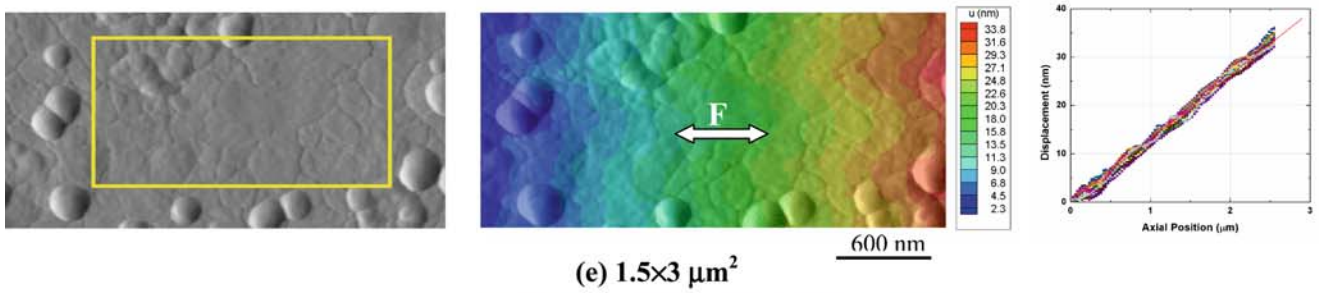

(e) 1.5×3 μm²

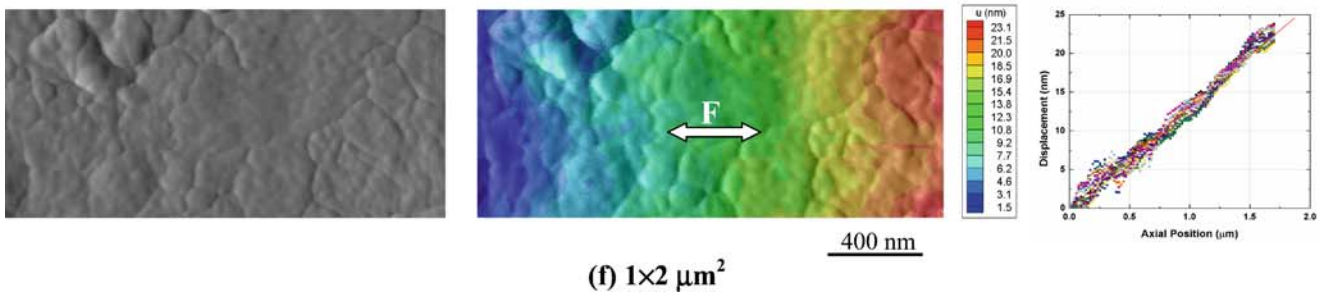

(f) 1×2 μm²

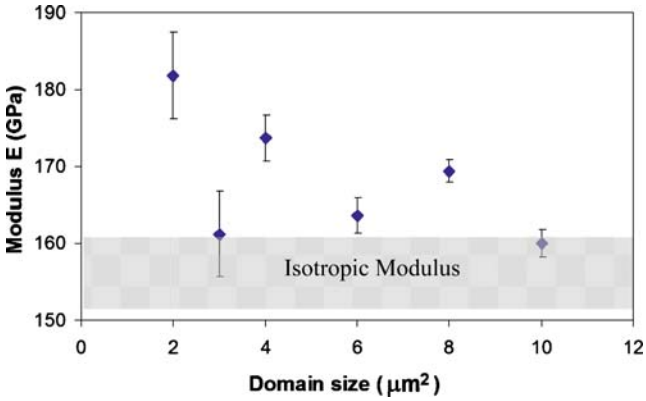

Fig. 7 Effective modulus as a function of domain size. The *error bars* are the standard deviation in the line plots in Fig. 6. The *shaded area* corresponds to the isotropic modulus varying by one standard deviation

3×6, 4×8, and 5×10 μm^2. In the second example three mutually inclusive domains with dimensions of 1×2, 2×4, and 5×10 μm^2 were imaged by the AFM.

For direct comparison of the results, the physical dimensions of the DIC correlation square were set approximately the same for all AFM image sizes. Large correlation squares averaged out local displacement variations and decreased the contribution of individual grains to the computed displacement field, while small correlation squares introduced local errors or lack of algorithm convergence as the speckle pattern provided by the intra-grain surface roughness may not have been sufficient to determine accurately the displacements of each material point. This optimal correlation square was determined iteratively and it was the smallest correlation square that allowed for convergence without artifacts for all AFM image sizes. For instance, in the second example presented here the correlation square of the 5×10-μm^2 AFM images was 20×20 pixels (200×200 nm^2), for 2×4-μm^2 images was 60×60 pixels (240×240 nm^2), and for 1×2-μm^2 images was 100×100 pixels (200×200 nm^2). Given the 650 ± 50 nm grain diameter of SUMMiT-IV polysilicon, the aforementioned correlation squares were approximately 1 / 3 of the diameter of a polysilicon grain.

Figure 6 (left) shows the reference AFM images with 1,024 pixels per line resolution. The superimposed u-displacement contours on the AFM images are also shown to identify correlations between local deformation and grain structure. The arrows point to the direction of the applied force. To the right, the local u-displacement as a function of axial specimen location is plotted for 16–20 lines of the displacement contours. For a direct comparison, all lines were translated to the origin of the coordinate system. The straight line in each plot is the average of the best-fit lines to all experimental displacements and its slope is used as a measure of the average strain in the specimen. The periodic steps in the line plots in Fig. 6(b) are experimental artifacts that were not filtered out to preserve the fine data scatter.

The combined displacement contour/AFM topographic image of the largest area shows linearly varying axial displacements according to linear elasticity. The smaller fields of view are associated with increasing non-uniformity in displacement distribution compared to the 5×10-μm^2 AFM image. The smaller specimen domains, 1.5×3 and 1×2 μm^2, demonstrated the highest scatter in the axial displacement distribution. The local deformations in Fig. 6(e),(f) follow the material microstructure. A more accurate picture is provided by the line displacement plots. In the large areas the latter are very linear. However, the deviation from linearity was pronounced in the smaller specimen areas being maximum in the 1×2-μm^2 domain. The correlation coefficient, R^2, for the line plots in Fig. 6 varied from 0.96–0.993 for the smallest and the largest image size, respectively. These values and the average slope of all displacement lines provide a measure of the deviation of the effective deformation of these specimen areas from that of an RVE. For the purposes of this analysis the average slope of all displacement lines in each contour is used as a measure of the average strain in the sample as well as the local deformation inhomogeneity. Given this average strain value and the applied far-field stress, the effective elastic modulus in each field of view is computed. This quantity is finally used to determine the deviation of each specimen domain from the RVE whose effective mechanical behavior is characterized by the effective material modulus. The applied stresses values for each image size in Fig. 6(a–f) were 1.94, 2.1, 2.02, 2.18, 2.11, and 2.39 GPa, and the average strains computed from the line plots were 0.0121, 0.0124, 0.0123, 0.0125, 0.0131, and 0.0132, respectively.

The moduli computed from Fig. 6(a–f) and the standard deviations are plotted in Fig. 7. The shaded area designates the isotropic modulus bracketed by one standard deviation as measured from a large number of specimens using the AFM/DIC method in 5×15 μm^2 material domains. The calculated effective modulus varied with the domain size demonstrating a systematic trend to the isotropic behavior. The maximum standard deviation was computed for the smallest domain size while it became minimum for the largest domain size. The modulus trend towards the effective behavior was not monotonic. There were small domains (1.5×3 μm^2) whose effective mechanical response was closer to that of an RVE and

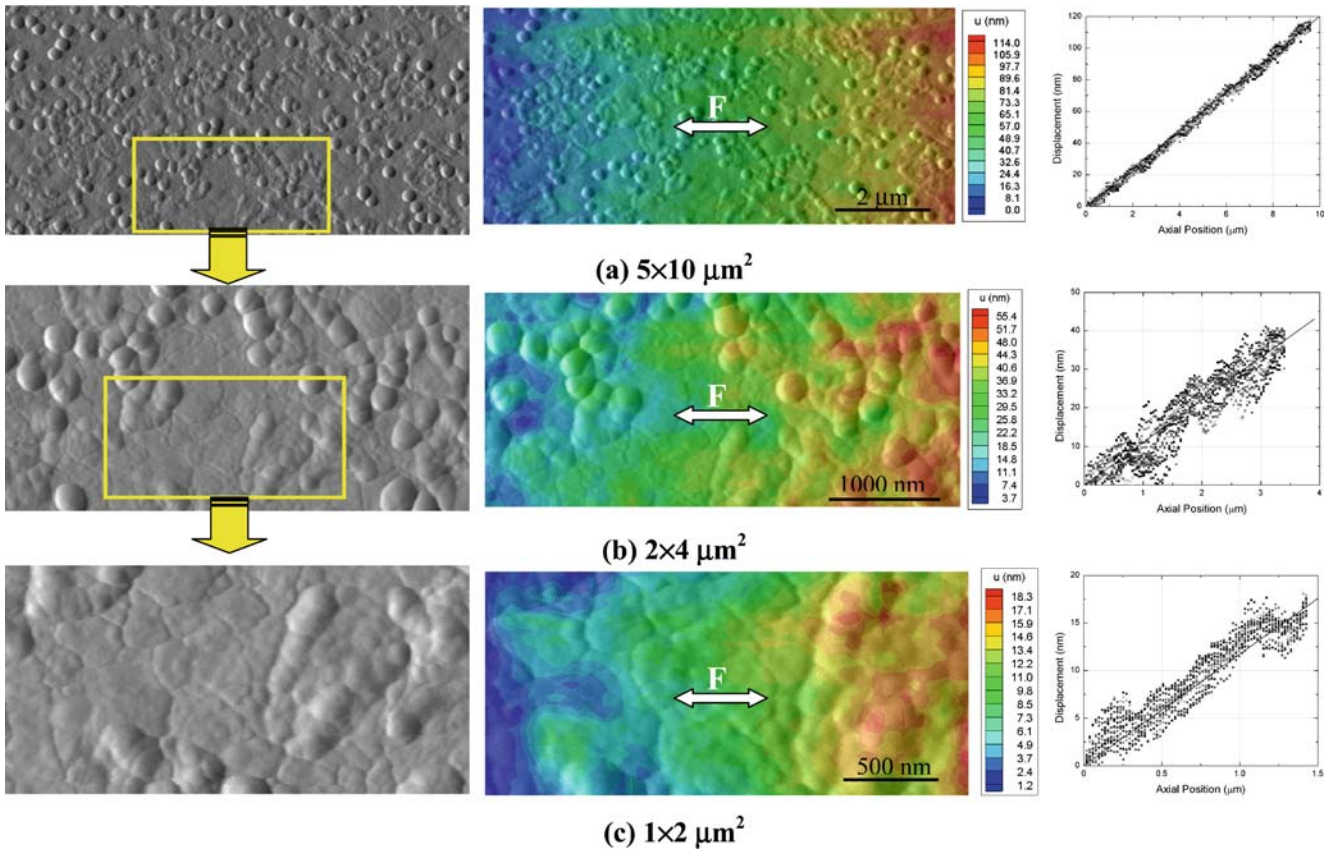

Fig. 8 (*Left*) AFM images of (**a**) 5×10 μm^2, (**b**) 2×4 μm^2, and (**c**) 1×2 μm^2 areas in a 2.5 μm thick polycrystalline silicon specimen under uniaxial tension. The areas marked by *rectangles* in (**a**) and (**b**) are images (**b**) and (**c**), respectively. All AFM images have 1,024 pixels per line resolution. (*Center*) *u*-displacement contours superposed on the grain structure. There is a direct correlation between local displacements and grain inhomogeneity for (**b**) 2×4 μm^2, and (**c**) 1×2 μm^2 areas. (*Right*) Plots of the local displacement as a function of position for each material domain extracted from the contour plots. The *straight lines* show the RVE behavior and are not data fit lines

relatively larger domains (2×4 μm^2) with larger deviation from the effective behavior. The minimum specimen area that provided an effective elastic modulus within the bounds of our measurements from the 5×15 μm^2 material domains was equal to 5×10 μm^2. The elastic modulus measured from the contour in Fig. 6(a) was 160 ± 2 GPa, which agreed with the value in Table 1 (155 ± 6 GPa). As a consequence a 5×10-μm^2 specimen area could be considered an RVE for polysilicon. This RVE size was confirmed by additional measurements on SUMMiT-IV polysilicon.

The plots in Fig. 6 provided a rather conservative picture of the effect of material inhomogeneity. An example of local displacements that deviate significantly from a uniform distribution is provided in Fig. 8. Three image sizes with dimensions 1×2-, 2×4-, and 5×10-μm^2 were employed. Contrary to Fig. 6(a), the displacement non-uniformity in 2×4 and 1×2-μm^2 domains in Fig. 8(b) and (c) was pronounced as local grain inhomogeneity considerably affected the displacement distribution. A quantitative description of the variation of local displacements in the three AFM image sizes is given by the line plots Fig. 8(a–c) that show 24, 18, and 17 displacement lines from each contour in Fig. 8(a–c), respectively.

The displacement lines in Fig. 8(a) have relatively constant slope and thus the strain is uniform. The elastic modulus calculated from the contour in Fig. 8(a) was 155 ± 2 GPa that agreed with the value in Table 1 which implies that the 5×10-μm^2 specimen area was larger than or equal to the RVE. On the contrary, the smaller areas in Fig. 8(b) and (c) showed significant displacement nonlinearity. Using the applied stress for each image size, 1.83, 2.06, and 2.75 GPa, and the effective elastic modulus from Table 1, the average strain in the three domains sizes in Fig. 8(a–c) should have been equal to 0.0117, 0.0132, and 0.0176, respectively. The displacement lines corresponding to these strains (slopes) are plotted in Fig. 8(a–c) to demonstrate the deviation from material homogeneity. A calculation of an effective modulus for the two small domains, i.e., 1×2, 2×4 μm^2, yielded 196 ± 22 and 226 ± 15 GPa, respectively, that were not within the modulus bounds for single crystal silicon, i.e., $130.2 < E < 187.9$ GPa. This occurred because the displacement lines for the 1×2-, 2×4-μm^2 specimen

domains deviated significantly from linearity and thus a linear fit of the data is an appropriate approach. The correlation coefficient, R^2, a measure of local deformation inhomogeneity, varied between 0.898–0.968 for 1×2-μm^2, 0.875–0.981 for 2×4-μm^2, and 0.996–0.998 for the 5×10-μm^2 areas. In comparison, for the 5×15-μm^2 contour in Fig. 3 that was recorded under the same stress as the 5×10-μm^2 contour in Fig. 8(a), $R^2 = 0.9989$–0.9994 and $E = 157 \pm 3$ GPa. This agreement further supports the conclusion that the smallest RVE for polysilicon from the SUMMiT-IV process is 10×10 μm^2.

From this analysis it is concluded that the mechanical behavior of polysilicon samples equal or larger than 10×10 μm^2 is described by its effective properties. Given the 650 nm average grain size of SUMMiT polysilicon, a material domain that includes $15 \times 15 = 225$, or more, columnar grains behaves homogeneously with a statistical scatter of less than 5%. This experimental assessment of the RVE is in agreement with the computational results in [6] for polysilicon with <100> texture. It also provides a measure of the number of grains in the RVE rather than an absolute length scale, which may be used to obtain estimates for the physical size of an RVE of polysilicon with different grain size but the same grain structure and orientation distributions as the samples used here. Along the same lines were the results of the analysis in [24] which concluded that for many cubic materials the RVE is at most 20 times the grain size. It is characteristic that analogous results were obtained before for macroscopic polycrystals, such as columnar ice, with grain structure similar to polysilicon. Specifically, [25] showed that 300 grains are sufficient to bring the elastic modulus of S2 ice within the Voigt–Reuss bounds that are meaningful for a statistically homogeneous solid and thus 300 grains would constitute an RVE.

The description of specimen deformations under non-uniform stresses using isotropic properties deserves special attention, as larger domain sizes may be required to capture the smooth strain gradients in MEMS designs with acute notches or sharp corners. A previous report by this group has shown that the displacement field in a 15×15-μm^2 area next to a circular hole with a modest stress concentration factor of $K = 3$ and a diameter of 6 μm follows that described by the isotropic elastic constants [5]. The specimens were fabricated by the MUMPs 41 process and the grain size was half of that for SUMMiT polysilicon. Using the displacement field and the solution to the inverse hole problem, the Young's modulus and the Poison's ratio of MUMPs polysilicon were determined to be in very good agreement with those from uniform tension tests that are reported in Table 1. Furthermore, a study of the fracture of MUMPs polysilicon under mode I loading of mathematically sharp cracks [26] showed that 15×15-μm^2 experimental crack tip displacement fields compared well with the analytical solution assuming homogeneity and the elastic properties in Table 1. Thus, even in the presence of high strain gradients, the linear elastic constants can describe 15×15-μm^2, or larger, specimens sufficiently well. These results should be compared with the RVE for MUMPs polysilicon that could be inferred from the SUMMiT polysilicon measurements presented here. Using the calculated RVE size for SUMMiT polysilicon, the RVE for MUMPs polysilicon containing $15 \times 15 = 225$ grains is approximately 5×5 μm^2. Thus, the 15×15-μm^2 domains of MUMPs polysilicon used in the fracture and stress concentration measurements were larger than the RVE.

One should note that the assumed columnar grain structure in not perfectly regular because of grains that are oriented at non-zero angles with respect to the film normal. Thus, the actual material deformation is rather three-dimensional and the minimum RVE may be larger than estimated here. In any event, polysilicon domains that contain less than 15×15 grains should rather be described in terms of property bounds, or by employing a thorough description of the local anisotropic elastic behavior and not the isotropic elastic properties.

Conclusions

The variability in the elastic properties of polycrystalline silicon as a function of fabrication source was investigated. The effective elastic modulus and Poisson's ratio of MUMPs and SUMMiT polycrystalline silicon were very close, averaging 164 ± 7 and 155 ± 6 GPa, and 0.219 ± 0.02 and 0.224 ± 0.02, respectively. The effective modulus was determined from 5×15-μm^2 specimen areas and was in agreement with the modulus measured from cross-head displacements. The Poisson's ratio obtained from the same specimen domains agreed well with a previous literature report for MUMPs polysilicon using significantly larger specimens that assured statistical homogeneity. On the contrary, the average mechanical strength of MUMPs polysilicon was found to be only 60% of SUMMiT polysilicon, being influenced by the increased surface roughness.

It was experimentally shown that the effective isotropic properties could be used to predict the deformation of 10×10-μm^2 specimen sizes, or in general polysilicon domains that include 15×15 columnar grains with no particular preference in texture. Using this result for SUMMiT polysilicon, the RVE for MUMPs polysilicon

was estimated to be 5×5 μm^2. For smaller specimen sizes the predicted and the experimentally determined effective axial deformations were significantly different. As a result, the deformation of polysilicon components with less than 15×15 grains is more reliably described in terms of property bounds. Based on prior experimental data it was concluded that even in the case of non-uniform stresses or high strain gradients a 15×15 μm^2 MUMPs polysilicon specimen domain comprised of approximately 45×45 grains, was adequately described using the isotropic elastic constants.

These results point to the realization that MEMS devices with features smaller than 5 μm (MUMPs) or 10 μm (SUMMiT) may demonstrate very different effective mechanical behavior compared to their larger counterparts. Furthermore, the measurements presented here assumed well-developed columnar structure which is present in 1–2 μm thick polysilicon but not in the first 200 nm of the film where the grains are rather equiaxed [1]. As a consequence, polycrystalline anisotropy is expected to be important in nanoelectromechanical systems (NEMS). Because of their submicron size, the performance characteristics of NEMS that depend on local stiffness, e.g., resonance frequency, are greatly affected by local property variations. In the presence of polycrystallinity their mechanical performance must be described in statistical rather than deterministic terms.

Acknowledgments The authors gratefully acknowledge the support by the Air Force Office of Scientific Research (AFOSR) through grant F49620-03-1-0080 with Dr. B.L. Lee as monitor, and the support by the National Science Foundation (NSF) under grant CMS-0515111. The authors thank Dr. Thomas Buchheit from the Sandia National Labs for providing the SUMMiT-IV specimens.

References

1. Chasiotis I, Knauss WG (2003) Experimentation at the micron- and submicron scale. In: Gerberich W, Yang W (eds) Comprehensive structural integrity vol. 8. Interfacial and nanoscale failure. Elsevier Science, pp 41–87.
2. Sharpe WN Jr, Yuan B, Edwards RL (1997) A new technique for measuring the mechanical properties of thin films. J Microelectromechanical Syst 6(3):193–199.
3. Jayaraman S, Edwards RL, Hemker KJ (1999) Relating mechanical testing and microstructural features of polysilicon thin films. J Mater Res 14(3):688–697.
4. Vlassak JJ, Nix WD (1992) A new bulge test technique for the determination of Young's modulus and Poisson's ratio of thin films. J Mater Res 7(12):3242–3249.
5. Cho S, Cárdenas-García JF, Chasiotis I (2005) Measurement of nano-displacements and elastic properties of MEMS via the microscopic hole method. Sens Actuators A Phys 120:163–171.
6. Mullen RL, Ballarini R, Yin Y, Heuer AH (1997) Monte Carlo simulation of effective elastic constants of polycrystalline thin films. Acta Mater 45(6):2247–2255.
7. Drugan WJ, Willis JR (1996) A micromechanics-based nonlocal constitutive equation and estimates of representative volume element size for elastic composites. J Mech Phys Solids 44(4):497–524.
8. Liu C (2005) On the minimum size of representative volume element: an experimental investigation. Exp Mech 45(3): 238–243.
9. Koester DA, Mahadevan R, Hardy B, Markus KW (2001) MUMPs design handbook. Revision 6.0.
10. Sniegowski JJ (1996) Multi-level polysilicon surface-micromachining technology: applications and issues. International mechanical engineering congress and exposition. Proceedings of the ASME aerospace division AD 52, pp 751–759.
11. Schriner H, Davies B, Sniegowski J, Rodgers MS, Allen J, Shepard C (1998) Sandia agile MEMS prototyping, layout tools, education and services program. 2nd international conference on engineering design and automation, Maui, Hawaii.
12. Hetherington DL, Sniegowski JJ (1998) Improved polysilicon surface – micromachined micromirror devices using chemical–mechanical polishing. Proc SPIE 3440:148–153.
13. Dyck CW, Smith J, Miller S, Russick E, Adkins C (1996) Supercritical carbon dioxide solvent extraction from surface – micromachined micromechanical structures. Proc SPIE 2879:225–235.
14. Jensen BD, de Boer MP, Masters ND, Bitsie F, LaVan DA (2001) Interferometry of actuated microcantilevers to determine material properties and test structure nonidealities in MEMS. J Microelectromechanical Syst 10(3):336–346.
15. Chasiotis I, Knauss WG (2002) A new microtensile tester for the study of MEMS materials with the aid of atomic force microscopy. Exp Mech 42(1):51–57.
16. Cho SW, Chasiotis I, Friedman TA, Sullivan J (2005) Direct measurements of Young's modulus, Poisson's ratio and failure properties of ta-C MEMS. J Micromechanics Microengineering 25(4):728–735.
17. Sutton MA, Wolters WJ, Peters WH, Ranson WF, McNeil SR (1983) Determination of displacements using an improved digital image correlation method. Image Vis Comput 1(3):133–139.
18. Knauss WG, Chasiotis I, Huang Y (2003) Mechanical measurements at the micron and nanometer scales. Mech Mater 35(3–6):217–231.
19. Chasiotis I (2004) Mechanics of thin films and microdevices. IEEE Trans Dev Mat Rel 4(2):176–188.
20. Nye JF (1985) Physical properties of crystals. Clarendon, Oxford, p 145.
21. Brantley WA (1973) Calculated elastic constants for stress problems associated with semiconductor devices. J Appl Phys 44(1):534–535.
22. Voigt W (1928) Lehrbuch der kristallphysik, 2nd edn. B.G. Teubner, Leipsig, pp 962–963.
23. Reuss A (1929) Berechnung der fliessgrenze von mischkristallen auf grund der plastizitätts-bediengung für einkristalle. Z Angew Math Mech 9(1):49–58.
24. Ren ZY, Zheng QS (2002) A quantitative study of minimum sizes of representative volume elements of cubic polycrystals – numerical experiments. J Mech Phys Solids 50:881–893.
25. Elvin AA (1996) Number of grains required to homogenenize elastic properties of polycrystalline ice. Mech Mater 22:51–64.
26. Chasiotis I, Cho SW, Jonnalagadda K (2006) Fracture toughness and subcritical crack growth in polycrystalline silicon. J Appl Mech 73(5):714–722.